"Environmental Engineering" 10th International Conference
Vilnius Gediminas Technical University
Lithuania, 27–28 April 2017
http://enviro.vgtu.lt

eISSN 2029-7092 / eISBN 978-609-476-044-0

Article ID: enviro.2017.001
DOI: https://doi.org/10.3846/enviro.2017.001

Microseismic Monitoring of Hydraulic Fracturing – Data Interpretation Methodology with an Example from Pomerania

Michał Antoszkiewicz[1], Mateusz Kmieć[1], Paweł Szewczuk[1], Marek Szkodo[1], Robert Jankowski[2]

[1]*Faculty of Mechanical Engineering , Gdańsk University of Technology, Gdańsk, Poland*
[2]*Faculty of Civil and Environmental Engineering, Gdańsk University of Technology, Gdańsk, Poland*
E-mails: [1]michal.antoszkiewicz@pg.gda.pl

Abstract. Microseismic monitoring is a method for localizing fractures induced by hydraulic fracturing in search for shale gas. The aim of this paper is to conduct the data interpretation of the microseismic monitoring based on the results from Pomerania region of Poland. The data has been collected from an array of geophones deployed on the surface. Ground vibrations have been recorded and analyzed for fracture location, magnitude and breakage mechanism. A velocity model of underlying formations has been used for successful microseismic monitoring. The model has been further tuned with signal from perforation shots of known location. Imaging of events has been done using software MicSeis, which utilizes diffraction stacking of waveforms from multiple stations to image microseismic events with low signal-to-noise ratio. The imaging of microseismic events in MicSeis uses a grid search over all possible origin times and locations in the selected rock volume. The seismic moment tensors are automatically determined from the amplitudes from the grid search procedure and are used to model polarities of events which then enhance constructive interference. Function characterizing a maximum stack per time sample have been calculated over whole volume and analyzed using the STA/LTA algorithm. Once the event has been detected in time, location has been determined through analysis of the 3D spatial image function. The procedure has been used to detect five events during hydraulic fracturing in Pomerania.

Keywords: microseismic monitoring, hydraulic fracturing, surface array.

Conference topic: Environmental protection.

Introduction

Microseismic monitoring is a valuable tool for understanding the efficacy of hydraulic fracturing. The locations of microseismic events, with sufficient resolution, provide information on fracture geometry and properties (Phillips *et al.* 2002: 345–369; Warpinski *et al.* 1998: 335–346). In addition to location, source mechanisms of microseismic events provide advanced understanding of the fracturing process. For example, during the injection one can estimate the orientation and dimensions of hydraulic fractures from (hopefully reliable) real-time locations of microseismic events. After comprehensive analysis of the data collection, one can estimate stimulated reservoir volume as well as productivity (Mayerhofer *et al*. 2010: 16–18). Real-time monitoring can prevent fracturing outside the perspective zone and therefore prevent ground water pollution.

The most important step of signal analysis is the detection of the first arrival. In early days of microseismic monitoring signals from individual sensors were searched for characteristic symptoms of wave arrival either by qualified specialist or computer algorithm. One of the first of such algorithms was STA/LTA (short-term average/long-term average). It was a simple method comparing signal averaged over short period to signal averaged over long period (Allen 1978: 1521–1532). The algorithm was simple enough to be implemented on a single microcontroller for a real-time analysis. In the year 1987 Bear and Kradolfer proposed an extension of the STA/LTA algorithm. Method was supposed to detect P wave arrival by computing an envelope function and filtering of the signal. The following group of algorithms is based on the analysis of abrupt changes in signal parameters. An example of such parameter can be energy, which changes are analysed in Coppens' (Coppens 1985: 1212–1231) and modified Coppens' (Sabbione *et al*. 2010: V67–V76) methods.

As we drill deeper in search for oil and gas, microseismic waves get more and more attenuated by the overlaying formations. Because of that, in many cases, wave arrival cannot be picked in an individual record due to signal to noise ratio (SNR) lower than 1. In this case more sophisticated methods are used. Such methods benefit from cross correlation analysis, advanced filtering and statistical methods. They usually use some form of stacking of signal from multiple receivers, e.g. semblance stacking (Eaton *et al*. 2011: 1–4). As the microseismic signal, we search for, is common for all the receivers and noise is different in every location, stacking cancels out the noise and the useful signal gets amplified.

One of such methods is diffraction stacking (Gajewski *et al*. 2007: 5–7). The algorithm increases SNR by stacking records from multiple locations with appropriate shifting in time. This method can be further improved by accounting

for the polarity of the received signal. Signal polarity can be different for different receiver location and can degrade stacking affectivity due to destructive interference. To account for the signal polarity on the surface, source mechanism need to be determined. For this purpose one can use a method combining diffraction stacking with simultaneous source mechanism inversion (Zhebel 2015: KS1-KS9).

The method of diffraction stack with simultaneous source mechanism inversion was used to interpret microseismic data collected during 12-stage hydraulic fracturing of a horizontal well.

Monitoring overview

The monitored well is located in the north of Poland, Pomerania region. Additionally horizontal well is overlaid with formations that strongly distort the seismic signal: Cenozoic strata with very low wave propagation speeds and big attenuation factor and anhydrites sand salts which have a lot of fault plains causing refraction. The interfaces between salts and sandstones, which have high refraction factor, are also problematic.

The fracturing process consisted of 11 stages. Each stage preceded with 6 perforation shots. Additionally a string shot was performed with higher energy in nearby wellbore. As exact position and origin time is known for each of those events, they, if recorded by the surface array, enable us to improve ground velocity model by velocity model calibration.

Seismic signal was recorded by 40 patches distributed on a ground surface within 4 km radius from a projection of the well trajectory onto the ground level. Each patch consisted of 25 recording units. Each recording unit had a 12-geophone string connected to it and represented one recording channel. Patches were rectangular in shape with dimensions: 90×95 m. The patches were located denser in locations, where near surface low velocity layer is thinner. Additionally patches were not placed close to roads, in wooded area, wetland and urbanized locations.

Noise analysis

The first step of data analysis is noise analysis. Noise analysis is using computation of root-mean-square (RMS) values of real amplitudes in data for different time periods. Noise levels were evaluated during a weekend day (Sunday 05.06.2016) and a week day (Monday 06.06.2016) as it was found that these days were characteristic and we did not observe significant noise changes on the other days during the monitoring period. Figure 1 shows computed mean noise level for all the patches during 4 periods of a weekday.

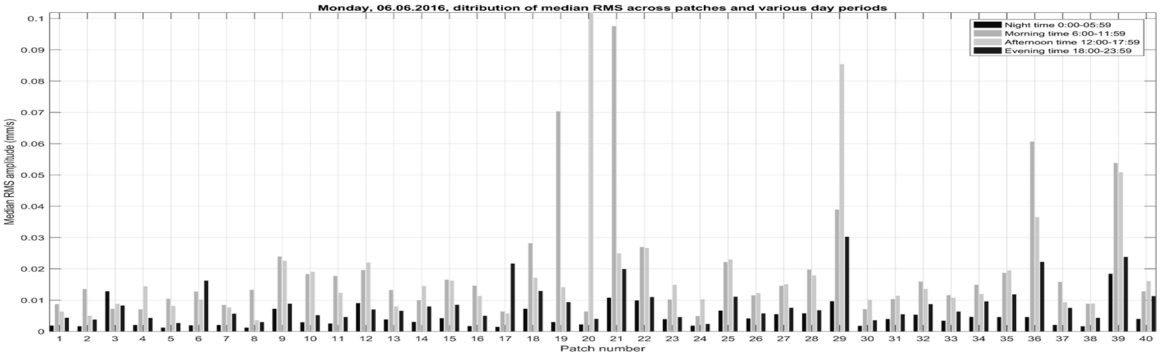

Fig. 1. Distribution of noise for all the patches during various periods of the weekday

Velocity model building

For correct event detection and localization, a velocity model is needed. The velocity model describes the velocity of seismic waves depending on depth with respect to mean sea level (MSL). Preliminary velocity model for stacking of seismograms corresponding to the string shot and for the perforation shots study has been derived from the provided well log information and is presented in Figure 2. The sonic log does not contain information on the shallow and deep part of the velocity model. This information was completed by an interpolation of the linear trend from the velocities at depths from 1800 to 3400 m and this trend was used to complete the velocity model at the bottom below 3,700 m. The top (near surface) part of the velocity model was approximated as a homogeneous velocity layer.

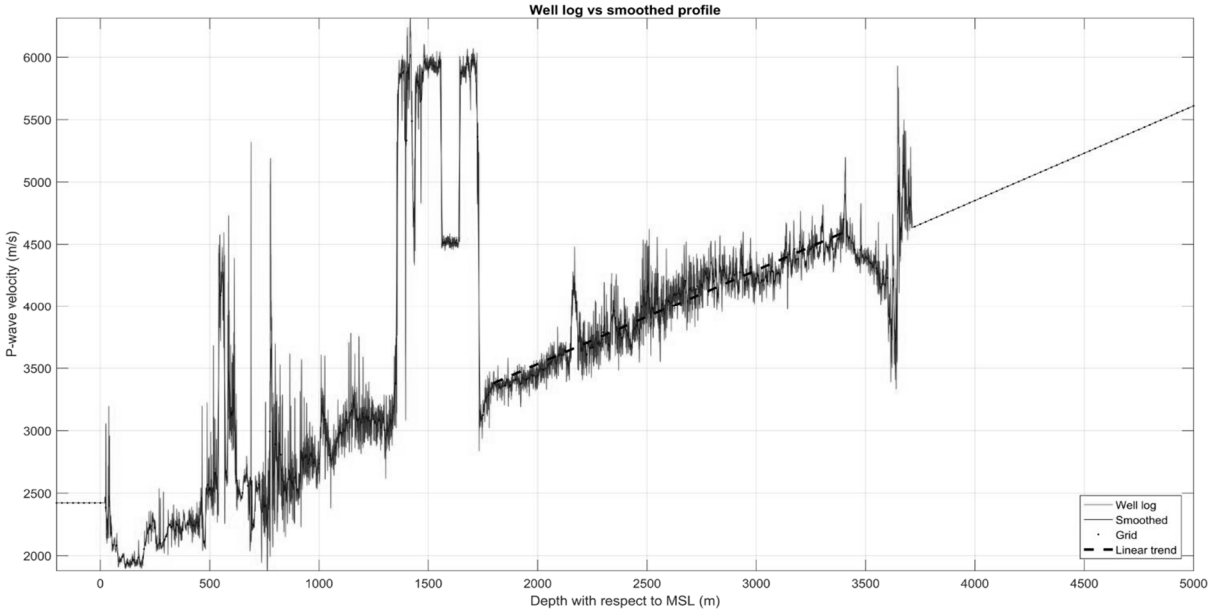

Fig. 2. Sonic log and its smoothed version. It represent the measured sonic log velocities. The dashed line represents the interpolated smoothed velocity model

Diffraction stacking procedure

For event detection a diffraction stacking procedure is used. Firstly one needs to discretize the subsurface. Only the zone in which the rock cracking is expected is considered (Fig. 3). We started with the preliminary velocity model obtained by smoothing of well log and interpolation to 25 m grid. Imaging zone size was 2.5×2.5 km in horizontal direction and 1.5 km in depth (Fig. 3). After discretizing the imaging zone, a set of image points was obtained.

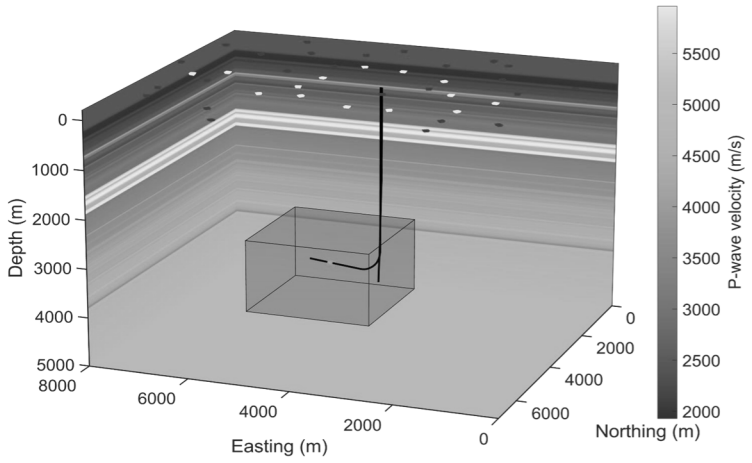

Fig. 3. Velocity cube, well path and selected volume for velocity model calibration: used patches (white), high noise patches not used for stacking (dark), imaging zone (cube)

Having the velocity model, travel times from each image point to each receiver were computed with ray tracing method. Seismic records were filtered prior to stacking using Butterworth bandpass filter from 20 to 40 Hz to reduce influence of low frequency noise and surface waves on the stack. For each source location (image point) and for each possible origin time the value of the stack function is computed by shifting signals from the receivers accordingly to the computed travel times and adding amplitude values:

$$S(x,y,z,t) = \sum_{R} A\left(t + t_P^R(x,y,z)\right), \tag{1}$$

where S is the computed stack value for the image point (x, y, z) and origin time t, A is the recorded seismogram, t_P^R is the computed P-wave travel time from the source point (x, y, z) to the receiver R on the surface.

SNR can be additionally improved by accounting for the polarity of the signal (Duncan 2010: 75A139; Zhebel, Eisner 2012: 1–5). To achieve that, the inversion of the moment tensor at each image point and origin time is needed. When computed moment tensor predicts negative wave polarity for a receiver then the corresponding amplitude is multiplied by –1.

After the 4-dimensional stack is computed, STA/LTA algorithm with predefined threshold is used to detect events. The location of the event $(\hat{x}, \hat{y}, \hat{z})$ is an image point in which the stack has the highest value. To compute event origin time the shortest travel time from image point $(\hat{x}, \hat{y}, \hat{z})$ is subtracted from the time corresponding to the highest stack value (Gajewski *et al*. 2007: 5–7).

Velocity model calibration

For better event detection and localization one shall calibrate the velocity model. For this process a seismic event with known location and origin time is needed. It is not any easy task since the magnitudes of the seismic events observed during the fracking works are relatively low and they can not be compared to tectonic earthquakes, often resulting in substantial damages (see, for example, Falborski, Jankowski 2013: 143–150; Jankowski 2007: 931–942, 2015: 1550012; Jankowski, Mahmoud 2016: 3075–3097; Naderpour *et al.* 2016: 1504783). In the case of fracking works, the candidates for such events are string and perforation shots. A diffraction stack was computed for all periods corresponding to the string shot but we were not able to obtain any reliable detection of the string shot. A few of the relatively high stack amplitude with higher STA/LTA corresponded to low semblance value. This indicates that these high stack values are most likely related to noise.

Other candidates for velocity model calibration are perforation shots. According to the journal of operations, there were 66 perforation shots in total during 11 fracturing stages. The visual inspection of 66 files corresponding to these origin times showed that there are no sign signal to noise arrivals consistent with body waves and several pre-processing steps are necessary together with appropriate filtration to identify perforations and calibrate the velocity model.

The noise analysis was performed so as to determine noise levels of time intervals corresponding to the perforations. This allowed us to select the most promising perforation shots for calibration and also select patches and receivers appropriate for stacking in each case. To test if the data contain sufficient signal we selected 11 patches nearest to the well head, applied band pass filtration (4th order Butterworth bandpass filer from 10 Hz to 40 Hz) and sorted the patches by increasing distance from well head. This allowed us to identify the surface waves associated with the perforation shots and stack signal preceding these waves to analyze the P-wave body wave. This methodology allowed us to identify the optimal data intervals and calibrate the velocity model.

The median noise levels for each file that contains perforation shot signal was estimated. Individual noise levels for each trace were computed as 90-ieth percentile of all absolute amplitudes in the trace. The lowest noise levels corresponded to perforation shot files recorded during the Stage 5. The second lowest noise levels were observed for the Stage 6 recorded during the same day (weekend) but later (18:00–19:00). Perforation shots 25–30 were also the earliest and hence they were the most possible candidates for calibration. For visual identification of surface waves related to the perforation shots, the patches which are situated within 2 km zone from the well head were only selected. The selected patches were sorted by increasing distance from the well head. An example of the recorded body P-wave and the corresponding surface waves of a perforation is shown in Figure 4.

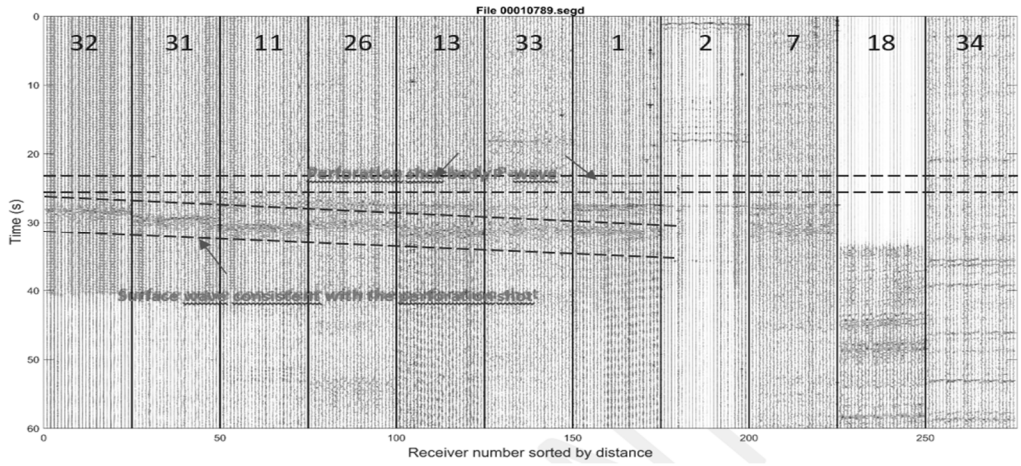

Fig. 4. Seismic traces for the patches (see the number of patch at the top of each section separated by the vertical blue lines) close to the well head for the period of the perforation shot 30

The delay across receivers is 0.04 s for receivers 78 meters apart. This gives apparent velocity of 1950 m/s, which seems to be consistent with perforation shot body P-wave.

We focused on imaging of the perforation shots from the Stage 5, as they provided the best signal to noise potential. An example of detection of the perforation 28 is shown in Figure 5.

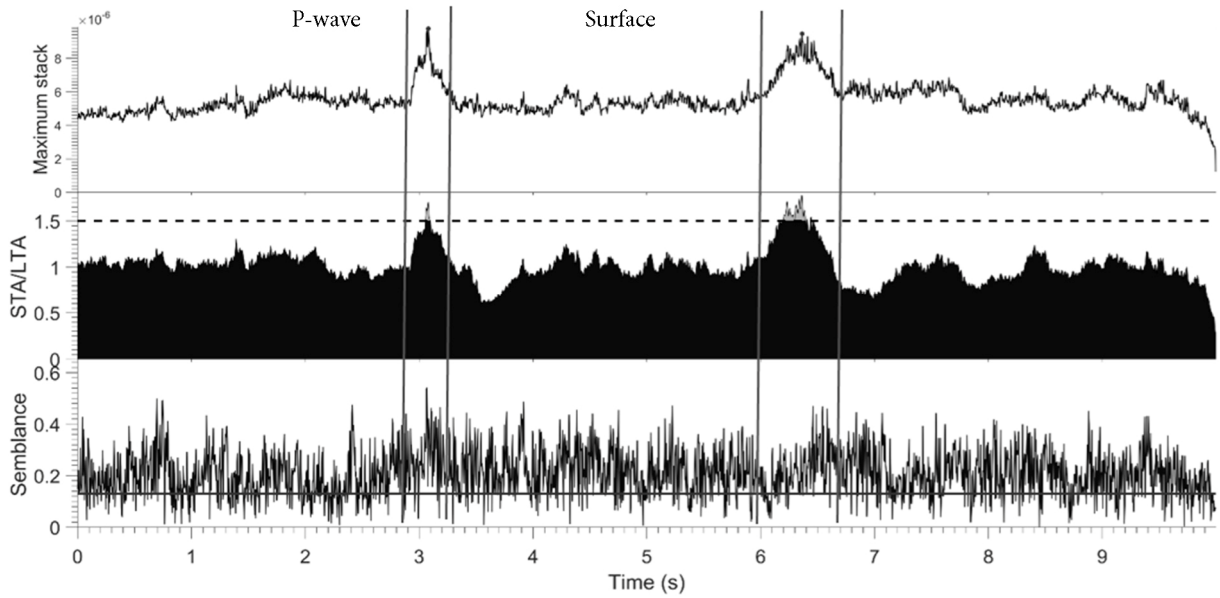

Fig. 5. Stack function (top plot), short-time-average to long-time-average ratio (STA/LTA) (middle plot) and semblance (bottom plot) corresponding to the perforation shot 28

Data were filtered prior to stacking using Butterworth bandpass filter from 20 to 40 Hz to reduce influence of low frequency noise and surface waves on stack. Only 14 patches with lowest noise were used for that purpose. The STA/LTA ratio of the direct P-waves is around peaking at 1.7 and the corresponding stack is high too. The surface wave arriving approximately 4 seconds after the P-wave also produces high stack but much lower semblance values corresponding to the peaks of the stack. The perforation shot location needs to be done only over the time interval corresponding to direct body P-wave and avoid the surface waves to avoid false detection and ensure correct calibration. The lateral deviation from true position of the perforation 28 is small, vertical locations are significantly different, the image in the uncalibrated model locates perforation approximately 600 m deeper. Vertical bias of 600 m deeper indicates that it is necessary to calibrate velocity model by increasing it to approximately 15% because 600 m is approximately 15% of total depth of the perforation from the surface level.

Perforations 25, 26, 27, 29 and 30 were the next imaged ones. The higher stack functions for perforations 25, 28 and 30 indicate that their locations are more reliable and they are more suitable for the velocity model calibration. Stack function for perforation 27 has too small SNR and this event could not be reliably imaged and is not used for velocity model calibration. Perforations 26 and 29 have less distinct stacks and reliability of their location is limited.

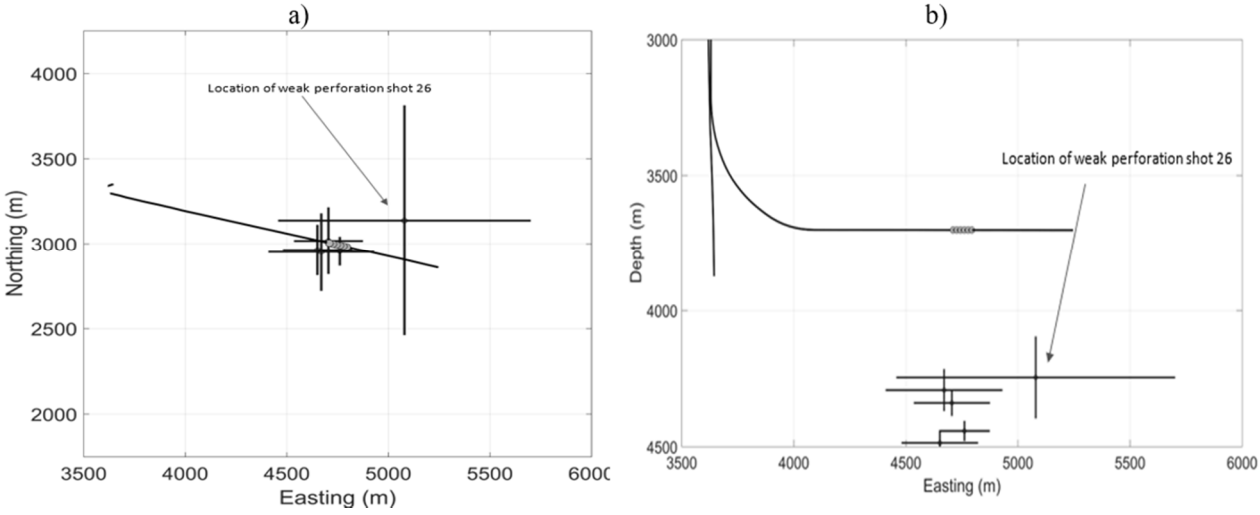

Fig. 6. A map view of locations for perforations 25, 26, 28, 29, 30 in the uncalibrated velocity model, a) horizontal view, b) vertical view

Figure 6 shows locations of the 5 well constrained perforation shots (25, 26, 28, 29, 30, respectively) from the stage 5 that were obtained with the uncalibrated model. We see from the figure that lateral positions of the located perforations agree with their true positions within the error of the location. However, an average vertical bias for the group of the selected perforations is approximately 600 m. We applied a constant 15% bulk shift increase of the whole velocity model, i.e. increased velocity at every grid node by 15%. The locations of the perforations in the newly calibrated velocity model are shown in Figure 7. Note that the images perforations in the calibrated model are closer to the true locations. The four beat located perforations have vertical misfit less than 200 m. The true locations are within the uncertainties of determined locations for all five perforations. The weakest perforation 26 has the biggest mistfit. The depth difference of the best determined perforation differs only by 15 m from the true depth.

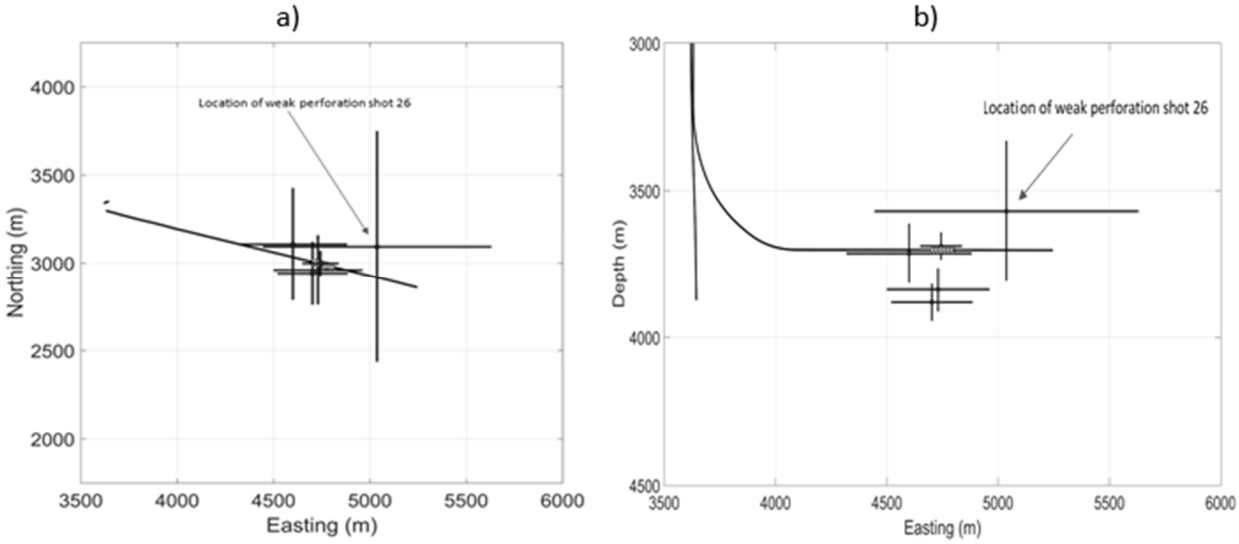

Fig. 7. A map view of locations for perforations 25, 26, 28, 29, 30 in the calibrated velocity model, a) horizontal view, b) vertical view

Conclusions

It was difficult to detect any seismic events by diffraction stacking method due to great vertical depth of the well and problematic overlaying formation. It is believed that synchronization of surface and downhole array may lead to detecting seismic events related to hydraulic fracking. Additionally we did not have velocity model for shallow and deep formation and the interpolation of the data was needed. Ideally, a 3D seismic migration model would overcome the lack of the velocity information at the near surface with more realistic velocities and possibly better detection and location of microseismic events.

Unfortunately, string shot was too weak to calibrate the velocity model. It does not allow determination of statics and velocity calibration in general. We recommend to use either stronger string shot at the same depth or several similar size shots at shallower depths to provide a better constraint on statics and velocity model calibration. This information is crucial for successful calibration detection and location of microseismic events. Perforation shots resulted in stronger SNR and allows calibration of the velocity model but it does not allow for determination of statics. The final calibrated velocity model is 15% faster than smoothed model based on sonic log.

Acknowledgements

The research work was funded by the National Centre for Research and Development in Poland under the project no. BG1/GASŁUPMIKROS/13 (programme Blue Gas – Polish Shale Gas). This support is greatly acknowledged. The authors would also like to thank AGH University of Science and Technology for help in surface array design and sharing of event data from downhole monitoring, Geofizyka Toruń SA company for the realization of field operations, Seismik s.r.o., especially Leo Eisner and Denis Anikiev, for data analysis, PGNiG SA company for geophysical data and cooperation.

References

Allen, R. V. 1978. Automatic earthquake recognition and timing from single traces, *Bulletin of the Seismological Society of America* 68(5): 1521–1532. Prieiga per internetą: http://www.bssaonline.org/content/68/5/1521.short

Coppens, F. 1985. First Arrival Picking on Common-Offset trace collections for automatic estimation of static corrections,

Geophysical Prospecting 33(8): 1212–1231. https://doi.org/10.1111/j.1365-2478.1985.tb01360.x

Duncan, P. M.; Eisner L. 2010. Reservoir characterization using surface microseismic monitoring, *Geophysics* 75(5): 75A139. https://doi.org/10.1190/1.3467760

Eaton, D. W.; Akram, J.; St-onge, A.; Forouhideh, F. 2011. Determining microseismic event locations by semblance-weighted stacking, *CSEG Annual Convention*: 1–4.

Falborski, T.; Jankowski, R. 2013. Polymeric bearings – a new base isolation system to reduce structural damage during earthquakes, *Key Engineering Materials* 569–570: 143–150. https://doi.org/10.4028/www.scientific.net/KEM.569-570.143

Gajewski, D. J.; Anikiev, D.; Kashtan, B.; Tessmer, E.; Vanelle, C. 2007. Source Location by Diffraction Stacking, in *69th EAGE Conference and Exhibition Incorporating SPE EUROPEC 2007*: 5–7. https://doi.org/10.3997/2214-4609.201401879

Jankowski, R. 2007. Theoretical and experimental assessment of parameters for the non-linear viscoelastic model of structural pounding, *Journal of Theoretical and Applied Mechanics* 45(4): 931–942.

Jankowski, R. 2015. Pounding between superstructure segments in multi-supported elevated bridge with three-span continuous deck under 3D non-uniform earthquake excitation, *Journal of Earthquake and Tsunami* 9(4), 1550012. https://doi.org/10.1142/S1793431115500128

Jankowski, R.; Mahmoud, S. 2016. Linking of adjacent three-storey buildings for mitigation of structural pounding during earthquakes, *Bulletin of Earthquake Engineering* 14(11): 3075–3097. https://doi.org/10.1007/s10518-016-9946-z

Mayerhofer, M. J.; Lolon, E., Warpinski, N. R.; Cipolla, C. L.; Walser, D. W.; Rightmire, C. M. 2010. What is stimulated reservoir volume?, *SPE Production & Operations* 25(1): 16–18. https://doi.org/10.2118/119890-PA

Naderpour, H.; Barros, R. C.; Khatami, S. M.; Jankowski, R. 2016. Numerical study on pounding between two adjacent buildings under earthquake excitation, *Shock and Vibration* 2016: article ID 1504783. https://doi.org/10.1155/2016/1504783

Phillips, W.; Rutledge, J. T.; House, L. S.; Fehler, M. C. 2002. Induced microearthquake patterns in hydrocarbon and geothermal reservoirs: six case studies, *Pure and Applied Geophysics* 159(1): 345–369. https://doi.org/10.1007/PL00001256

Sabbione, J. I.; Velis, D. 2010. Automatic first-breaks picking: New strategies and algorithms, *Geophysics* 75(4): V67–V76. https://doi.org/10.1190/1.3463703

Warpinski, N. R.; Branagan, P. T.; Peterson, R. E.; Wolhart, S. L.; Uhl, J. E. 1998. Mapping hydraulic fracture growth and geometry using microseismic events detected by a wireline retrievable accelerometer array, *SPE Gas Technology Symposium*: 335–346. https://doi.org/10.2118/40014-MS

Zhebel, O.; Eisner, L. 2015. Simultaneous microseismic event localization and source mechanism determination, *Geophysics* 80(1): KS1-KS9. https://doi.org/10.1190/geo2014-0055.1

Zhebel, O.; Eisner, L. 2012. *Simultaneous microseismic event localization and source mechanism determination*. SEG Technical Program Expanded Abstracts 2012: 1–5. https://doi.org/10.1190/segam2012-1033.1